Optics and Lasers in Engineering 136 (2021) 106283

Contents lists available at ScienceDirect

Optics and Lasers in Engineering

journal homepage: www.elsevier.com/locate/optlaseng

Prism-assisted achromatic diffraction system for multi-focus biological microimaging

Haidong Zhang[a,b,c], Ruoqiu Wang[a], Xiaolin Yin[a], Xiaokun Wang[a,b,*], Xu Yang[d], Zhiyu Zhang[a,b,*]

[a] Changchun Institute of Optics, Fine mechanics and Physics, Chinese Academy of Science, Changchun 130033, China
[b] Center of Materials Science and Optoelectronics Engineering, University of Chinese Academy of Sciences, Beijing 100049, China
[c] Department of Electrical and Computer Engineering, National University of Singapore, Engineering Drive 3, Singapore 117576, Singapore
[d] School of Mechanical and Aerospace Engineering, Jilin University, Changchun 130025, China

ARTICLE INFO

Keywords:
Multi-focus microscope
Diffraction optical element
Chromatic aberration correction
Microscope imaging

ABSTRACT

Multi-focus microscope, which images multiple object planes of the sample simultaneously with a single shot, can significantly enlarge the observation depth and improve the time resolution of the microscope. Conventional multi-focus microscopes are quite bulky and the achromatic methods can only work for a single multi-focus diffraction lens. To solve this problem, equilateral triangular prisms (ETPs) are employed to correct the chromatic aberration generated by the multi-focus diffraction lens. This achromatic method can cope with a variety of multi-focus lenses with different parameters, which is significant to reduce the system complexity and improve device usability. For the multi-focus lenses with focal length greater than 600 mm, the resolution reduction value can be controlled within 50 nm through the fused silica ETPs. Based on the experimental setup, three sharp images of different object planes can be captured simultaneously by the detector. The resolution and imaging experiments demonstrate that the proposed scheme is reliable and flexible.

1. Introduction

Three-dimensional (3D) imaging for living specimens is still a challenge in biological research. Conventional microscopes, such as confocal laser scanning microscope, two-photon excitation microscope and wide-field microscope, acquire 3D images reconstructed by a stack of high lateral resolution images via scanning 2D images of different planes [1,2]. However, due to the relative long scanning time, it is hard to get a clear 3D image for moving objects by stitching together the 2D images taken at different times [3,4]. In addition, there is an intrinsic conflict between high power microscopy and large depth of field. When it is necessary to perform observations of living cells at large depth range in real time, conventional microscopes also cannot cope well due to the limited observation depth.

To overcome these limitations, the idea of multi-focus microscope was proposed [5–8]. The multi-focus microscope can capture multiple images from different object planes simultaneously with a single shot. Based on this idea, it can enlarge the observation depth of conventional microscope and also improve the time resolution for scanning microscope.

Many efforts have been taken to achieve multi-focus microimaging [9–11]. For example, beam splitters were employed to modify the emission pathway of a standard microscope, in which two focal planes can be achieved simultaneously [12–14]. Moreover, a large field of view and a high energy efficiency could be obtained by this method. However, the optical system of this method is quite complex and bulky if more focal planes are captured simultaneously. In addition, it is not applicable in practice if a detector is required for each optical branch in the system configuration.

Diffraction optical lenses were firstly introduced in the microscope to achieve multi-focus imaging by Blanchard et al. [15,16]. Utilizing a three-focus diffraction lens, the microscope can simultaneously capture three images from different object planes by one detector with a single shot. However, since diffraction lens has strong chromatic aberration at nonzero diffraction orders, multi-focus microscopes can only work at a single wavelength or extremely narrow bandwidth without dispersion correction.

In 2013, Sara Abrahamsson et al. proposed an aberration-corrected multi-focus microscope based on the achromatic combination of a grating and an optical wedge to obtain nine-focus microimaging [17]. In the microscope, a green 515/30 nm emission filter was used and the diffraction efficiency for the multi-focus lens is 65% with even distribution between images. However, it is inconvenient in practice that the achromatic grating needs to be specially designed for each multi-focus lens of different focal length interval. Moreover, the achromatic grat-

* Corresponding author.
E-mail addresses: jimwxk@sohu.com (X. Wang), zhangzhiyu@ciomp.ac.cn (Z. Zhang).

https://doi.org/10.1016/j.optlaseng.2020.106283
Received 19 March 2020; Received in revised form 20 May 2020; Accepted 14 June 2020
Available online 24 July 2020
0143-8166/© 2020 Elsevier Ltd. All rights reserved.

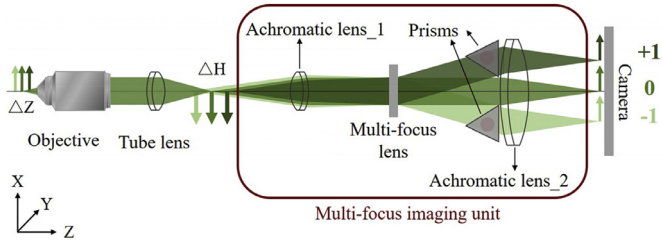

Fig. 1. The schematic layout of multi-focus microscope.

ing decreases the energy collection efficiency, which is critical at low excitation light dose.

In this paper, we developed a novel aberration-corrected multi-focus microscope based on the principle of the opposite dispersion in refraction and diffraction lenses. The equilateral triangular prism (ETP) are employed to correct the chromatic aberration generated by the multi-focus lens. It is more applicable compared with the above-mentioned achromatic methods. For the multi-focus lenses of different parameters, the optimum inverse dispersion can be obtained by rotating the angle of the ETP to compensate the chromatic aberration. However, since the chromatic aberration cannot be completely compensated by the equilateral triangular prism, there is still a small reduction in resolution (around 100 nm). This method is suitable for the observation scene with some redundancy in resolution, and not suitable for the observation scene where the characteristic size of the sample is very close to the limit resolution of the microscope.

In Section 2, the principle of this method is explained in detail. In Section 3, the critical multi-focus imaging unit is described in detail, including the multi-focus lens and ETP. In Section 4, resolution experiment and multi-focus microimaging experiments are conducted to demonstrate the feasibility of this scheme, and the aberration-correction characteristics of the prism and some limitations of this arrangement are discussed.

2. Proposed method

As schematically illustrated in Fig. 1, the multi-focus imaging unit is attached to a common microscope system. The multi-focus unit is mainly composed of a pair of achromats, multi-focus diffraction lens, ETPs and a detector. The sample is magnified by the microscope firstly, and the image produced by the microscope is captured again as an object by the multi-focus imaging unit. Two achromats form a 4F optical system, and the multi-focus lens is placed at the Fourier plane of the 4F system to get a uniform amplification for images of different diffraction orders. After passing through the multi-focus lens, the light carrying the information of the object is divided into multiple beams. For the three-focus lenses used in this research, the energy of incident light is evenly distributed in the +1, 0, −1 diffraction orders. The three-focus lens acts as a positive lens, a parallel plate, and a negative lens in the corresponding diffraction order, respectively. This makes the different parts of the detector correspond to three different object planes.

Based on the opposite dispersion between the diffraction and refraction elements, the ETPs are utilized to correct the chromatic aberration generated by the multi-focus lens at nonzero diffraction orders. Since the dispersion of the ETP is related to the incident angle of the light in addition to the material, the optimal achromatic effect can be obtained by tuning the placement angle of prisms.

Due to chromatic aberration correction, multiple object planes can be imaged sharply by the detector with a single shot. The multi-focus optical unit can deepen the observation range and improve the scanning efficiency of conventional microscopes.

3. Multi-focus imaging unit

3.1. Design of multi-focus lens

The conventional multi-step Fresnel zone plate usually distributes the main energy of incident light into its +1 diffraction order, and the energy distribution between low diffraction orders is not uniform. This results in non-uniform brightness of multiple images and image contrast reduction. In this research, a multi-focus lens was proposed, in which the energy of incident light can be distributed into multiple diffraction orders uniformly by modifying its phase function.

According to the principle of optical path reversibility, it is assumed that a beam of parallel light is incident on the surface of the multi-focus lens along the direction of -Z [18,19]. The complex amplitude of the incident beam is expressed by

$$W_0(\rho) = \sqrt{I_0(\rho)}\exp\left[i\varphi_0(\rho)\right] \tag{1}$$

where ρ is the radial coordinate in the multi-focus lens plane. The phase function of the multi-focus lens can be expressed as follow:

$$\varphi(\rho) = \Phi\left[\varphi_{MF}(\rho)\right] - \varphi_0(\rho)\ \rho \in [0, R] \tag{2}$$

where R is the radius of multi-focal lens. $\varphi_{MF}(\rho)$ is the wrapped phase function of lens with focal length f_{MF}. The corresponding paraxial phase is:

$$\varphi_{MF}(\rho) = \mathrm{mod}_{2\pi}\left(-\frac{k\rho^2}{2f_{MF}}\right),\ k = \frac{2\pi}{\lambda} \tag{3}$$

The phase function of transmitted beam can be modified as:

$$W(\rho) = \sqrt{I_0(\rho)}\exp\left\{i\Phi\left[\mathrm{mod}_{2\pi}\left(-\frac{k\rho^2}{2f_{MF}}\right)\right]\right\} \tag{4}$$

It is well known that any phase nonlinearity yields additional diffraction orders. In order to acquire the energy distribution of a series of foci, the phase function $\exp[i\Phi(\xi)]$ can be expanded into Fourier in the interval $\xi\in[0, 2\pi)$,

$$\exp\left[i\Phi(\xi)\right] = \sum_n a_n \exp(in\xi) \tag{5}$$

where

$$a_n = \frac{1}{2\pi}\int_0^{2\pi} \exp[i\Phi(\xi) - in\xi]d\xi \tag{6}$$

and

$$\sum_{n=-\infty}^{+\infty} |a_n|^2 = 1 \tag{7}$$

The following equation can be obtained by stitching Eq. (5) and Eq. (4):

$$W(\rho) = \sqrt{I_0(\rho)}\sum_n a_n \exp\left[-\frac{ik\rho^2}{2}\left(\frac{n}{f_{MF}}\right)\right] \tag{8}$$

The Eq. (8) is equal to a series of paraxial spherical beams with focal lengths

$$F_n = \frac{f_{MF}}{n} \tag{9}$$

and the corresponding energy proportion is calculated by $|a_n|^2$, n ∈ Z.

The relationship between the interval of adjacent object planes $\triangle Z$ (Fig. 1), the interval of relaying image plane $\triangle H$, and the magnification of the objective β can be expressed as follow:

$$\triangle Z = \triangle H/\beta^2 = {f_{Lens1}}^2/\left(f_{MF}\times\beta^2\right) \tag{10}$$

where f_{Lens1} is the focal length of the achromatic lens 1.

To ensure that multiple images can be completely imbedded without interference in the detector plane, it is necessary to introduce a proper tilted carrier frequency. The two critical conditions correspond to the fact that the image can be completely separated and fully accepted by

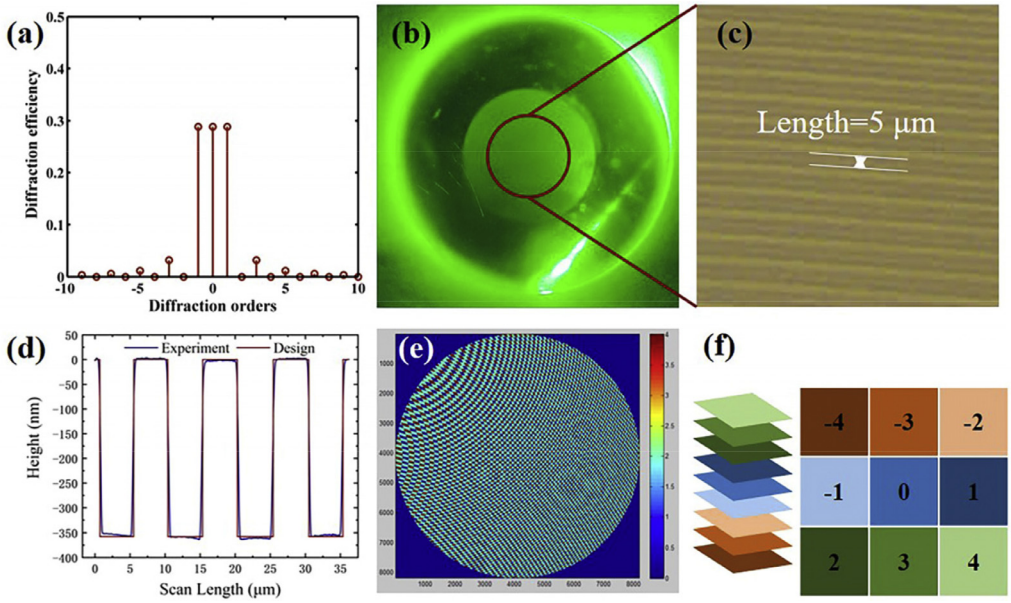

Fig. 2. Multi-focus lenses for microscope. (a) the energy distribution of three-focus lens. (b) photograph of the fabricated three-focus lens (c) optical micrograph in the central area of the three-focus lens (d) measured profile and design value of the fabricated lens (e) the phase map of the nine-focus lens. (f) the location of instant focal stack and images generated by the nine-focus lens.

the detector. The corresponding case can be expressed as the following system of equations,

$$\begin{cases} d\sin\theta = \lambda \\ \tan\theta = L/(3f_lens2) \end{cases} \tag{11}$$

$$\begin{cases} d\sin\theta = \lambda \\ \tan\theta = (3D - L)/6f_lens2 \end{cases} \tag{12}$$

where d is the center linewidth of multi-focus lens, L is the width of detector, D is the aperture of achromatic lens 2, and f_lens2 is the focal length of achromatic lens 2.

For the three-focus lens, the nonlinear transformation function $\Phi(\xi)$ can be defined in the following form:

$$\Phi(\xi) = \begin{cases} 0, \in [0,\ \pi) \\ 2\tan^{-1}(\pi/2), \in [\pi,\ 2\pi) \end{cases} \tag{13}$$

According to Eq. (6), it can be calculated that $|a_{-1}|^2 = |a_0|^2 = |a_1|^2 \approx 0.2885$. As shown in Fig. 2(a), an evenly distributed three diffraction orders can be generated with a total diffraction efficiency of 86.55% by a binary phase multi-focus lens. Fig. 2(b) is the photograph of the fabricated multi-focus lens under the guidance of this method. Fig. 2(c) shows the optical micrograph in the central area of this multi-focus lens, with a linewidth of 5 μm. By measuring the contour of the three-focus lens, we can find that the experimental and the design values maintain a high consistency (Fig. 2(d)). The design etching depth of the three-focus lens is 357 nm, which ensures the uniformity of brightness between the three images.

Even higher image acquisition efficiency can be achieved by combining two three-focus diffraction lens in the orthogonal direction. The phase map of nine-focus lens is shown in Fig. 2(e). Three different phases appear in the nine-focus lens and its diffraction efficiency is 74.91% (the square of the diffraction efficiency of the three-focus diffraction lens). The spatial distribution of the nine focal points and the corresponding images are shown in Fig. 2(f). Nine different object planes can be imaged simultaneously in a 3 × 3 matrix, which can greatly improve the time resolution of the scanning microscope.

3.2. Impacts of the fabrication errors

The diffraction patterns were directly written in a positive photoresist (Shipley 1805) spin-coated on a fused silica substrate via laser direct lithography system (DWL4000, Heidelberg Instrument). The minimum writing feature can be up to 0.6 μm. After hardbaking, the photoresist patterns were etched into the fused silica substrate using an Ar-ion beam etching machine (IBF1500, Neue Technologien).

Taking a multi-focus lens with the center linewidth of 5 μm as an example, the effect of fabrication errors on the lens performance was analyzed. There are mainly two kinds of fabrication errors: (a) depth error of steps caused by variation in resist exposure doses and non-uniform spin-coating of photoresist, and (b) width error of steps due to variation in resist exposure doses. Fig. 3(a) shows the diffraction efficiencies of orders ±1 & 0, and the standard deviation of images brightness as a function of the depth error of steps, while Fig. 3(b) presents the same result as a function of the width error of steps. The simulation results indicate that the depth error of steps has a stronger influence on the uniformity of images than the width error of steps. Since the depth error can be controlled in 10 nanometers during processing, the multi-focus lens with high brightness uniformity can be achieved.

3.3. Refraction index design of the ETP

The dispersion of an ETP depends on the material properties and the incident angle of the light. For better achromatic performance, the optical material of prism should be studied.

Table 1 shows the refractive indices of the three commonly used optical materials between 500 nm and 530 nm. By calculating the deflection angle differences caused by different incident angles within a bandwidth of 30 nm, as shown in Fig. 4, it can be found that the minimum deflection angle difference generated by the ETP of H-ZF12 is 0.718°, while that brought by the fused silica is 0.112°

For the three-focus lens with central linewidth of 5 μm, according to the grating equation: $d\sin\theta_m = m\lambda$, the parallel light has a deviation of 0.172° in the first diffraction order at the central wavelength of 515 nm and the bandwidth of 30 nm. The selection of ETP materials follows the two principles: (a) the minimum deflection angle difference generated by the prism should be less than that caused by the multi-focus

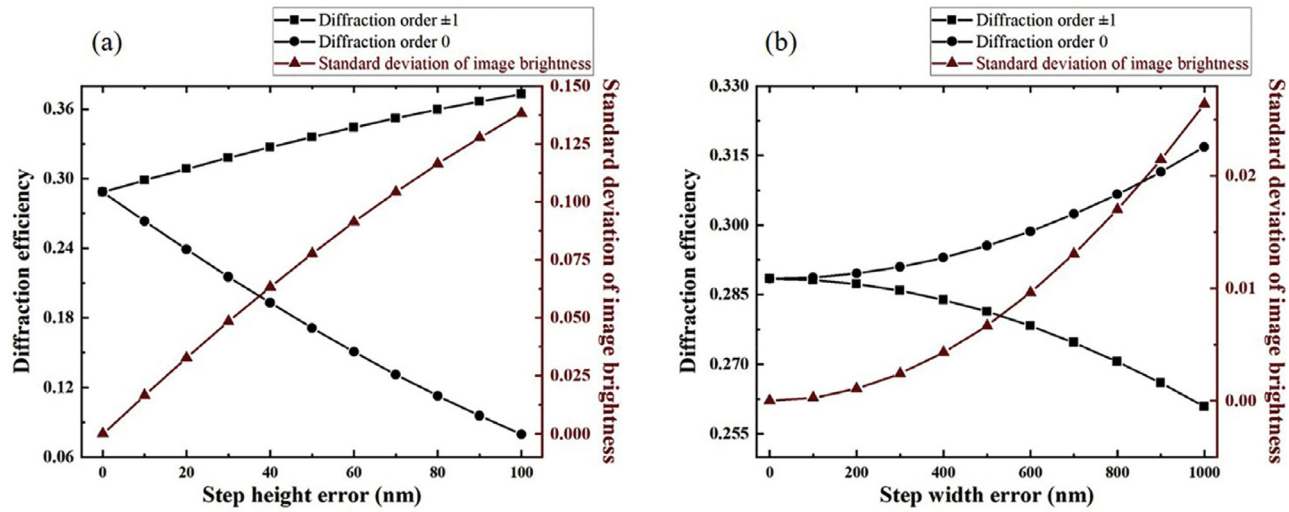

Fig. 3. Diffraction efficiencies and standard deviation of images brightness as function of (a) step height error and (b) step width error.

Table 1
Refractive indices of three optical materials.

Wavelength (nm)	500	505	510	515	520	525	530
BK7	1.5214	1.5211	1.5208	1.5204	1.5202	1.5199	1.5196
H-ZF12	1.8026	1.8012	1.8000	1.7987	1.7975	1.7964	1.7953
Fused Silica	1.4623	1.4621	1.4618	1.4615	1.4613	1.4610	1.4608

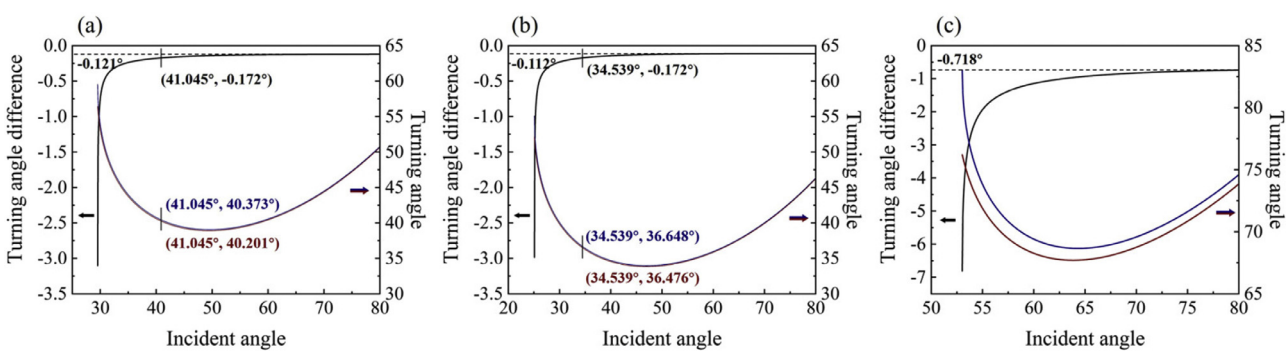

Fig. 4. The relationship between the turning angle and the differences and the incident angle within the bandwidth of 30 nm caused by the prism of (a) BK7, (b) fused silica, and (c) H-ZF 12.

lens. In this way, the chromatic aberration of the multi-focus lens can be compensated through the ETP; (b) the deflection angle brought by the prism is smaller for the same incident angle, which is conductive to the subsequent optical path adjustment.

In order to compensate the chromatic aberration of multi-focus lens used in the experiments, the turning angle caused by the BK7 prism is 40.373°, while that caused by the fused silica prism is 36.648°, as shown in Fig. 4(a) and (b). Combining the two factors above, the fused silica prism is selected to correct the chromatic aberration caused by the multi-focus lens.

4. Experimental results and discussion

4.1. Resolution experiments

To demonstrate the achromatic ability of the prism, a high-resolution transmissive test chart (HIGHRES-2, Newport) was used to quantitatively analyze the resolution of the multi-focus microscope. There are some opaque lines on the clear background of the test chart. A 50×, NA 0.6 objective with the theoretical resolution of 524 nm was used to magnify the sample. The illumination light in the experiments was a white light source and filtered by a 515/30 nm bandpass filter (FF01–515/30–25, Semrock). The focal length of the two achromatic lenses was 100 and 200 mm, respectively. A three-focus lens with a focal length of 266.66 mm and a central linewidth of 5 μm was located on the Fourier plane. As shown in Fig. 5(a), the resolution for zero diffraction order (no chromatic aberration generated by the multi-focus lens) is 548 nm (marked in red box), which is consistent with the theoretical value of the objective. If there is no achromatic prism, it can be found that the image of the resolution test chart at the first diffraction order has obvious chromatic aberration and greatly reduced the resolution (Fig. 5(b)). Moreover, the resolution in the meridian direction is much higher than that in the sagittal direction. This is due to the fact that the patterns of the three-focus lens are mainly distributed in the meridian direction, and thus the light has a significant dispersion in the sagittal direction.

In order to reduce the chromatic aberration, a fused silica ETP was employed in the light path of the first diffraction order. As presented in Fig. 5(c), an optimized achromatic image can be achieved by rotating the triangular prism. The resolution of the microscope at the first diffraction order is significantly improved. The resolutions along the meridian

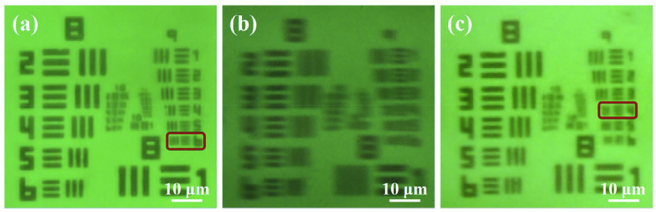

Fig. 5. The resolution of the multi-focus microscope. (a) 50× objective (NA 0.6) at zero diffraction order, and the optimal resolution is 548 nm as shown in the red box. (b) nonzero diffraction orders without aberration correction. (c) nonzero diffraction orders after aberration correction. The optimal resolution is 651 nm as shown in the red box.

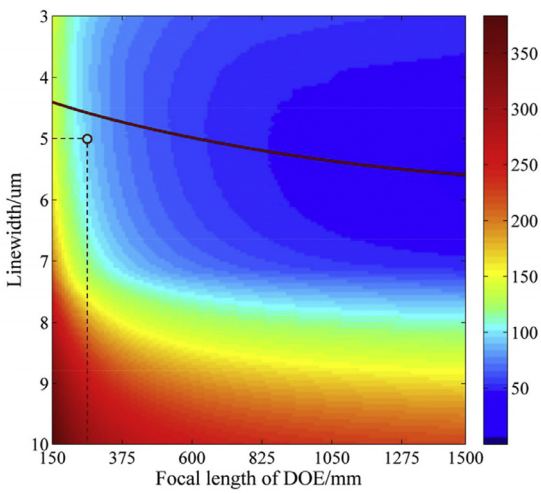

Fig. 6. The relationship between resolution reduction values and multi-focus lenses with different parameters. The optimal central linewidth is shown as the red line in the figure.

direction and sagittal direction keep the same. The optimal resolution is 651 nm, which means the residual chromatic aberration results in a 103 nm decrease in the resolution of the microimaging system.

After passing through the multi-focus optical unit, the ideal point light source on the relay plane forms a diffuse spot on the image plane. To verify the applicability of the prism to a series of multi-focus lenses with different parameters, the size of the diffuse spot was calculated by ray tracing method based on Snell's law and the grating equation. Fig. 6 shows the minimum resolution reduction caused by the residual chromatic aberration of multi-focus lenses with different focal lengths and center linewidths at the optimum prism angle. The multi-focus lens used in the resolution experiment (focal length = 266.66 mm, linewidth = 5 μm) was marked in the figure. The theoretical calculation result for resolution reduction is 100 nm, which is consistent with the experimental result.

For multi-focus lenses with different focal lengths, there exists an optimal central linewidth that minimizes the residual chromatic aberration after the achromatic process by the fused silica ETP. The optimal central linewidth is shown as the red line in the Fig. 6.

From the grating equation, we can know that the smaller the central linewidth of the diffraction element, the greater the chromatic aberration it generates. Therefore, it could produce greater residual chromatic aberration. When the central linewidth of the diffraction element becomes longer, the dispersion it brought is small. However, the inverse dispersion caused by the ETP has a minimum value, as discussed in Section 3.3. When the linewidth of the multi-focus diffraction lens further increases, the minimum inverse dispersion value of ETP is larger than that generated by the multi-focus lens. Thus, the influence of residual chromatic aberration on the resolution increases dramatically. When

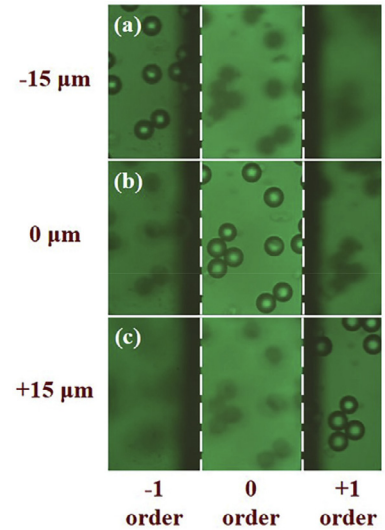

Fig. 7. Multi-focus imaging of silica microspheres with a diameter of 10 μm. The three columns correspond to the diffraction orders of −1, 0 and +1, respectively. The interval of two adjacent images is 15 μm.

the focal length of multi-focus lens is longer than 600 mm, the resolution reduction can be controlled within 50 nm.

Through calculation and analysis above, it can be found that this achromatic method has a wider applicability via tuning the angle of ETP, which does not need to be designed separately for the multi-focus lens.

4.2. Multi-focus microimaging experiments

To verify the imaging performance of the multi-focus microscope, transparent microspheres and human blood smear with object plan intervals of 15 and 5 μm were carried out.

4.2.1. Transparent microsphere

Transparent silica microspheres with a diameter of 10 μm are used as the samples. The microspheres are evenly distributed on a glass slide. The experimental setup and the three-focus lens are the same as that in Section 4.1. By slowly moving the stage, the sample passes through the three conjugated planes in turn from far to near. The corresponding dynamic video (Supplementary Material 1) is recorded by the detector and three key frames of the video are presented in Fig. 7. Three independent images, corresponding to −1, 0 & +1 diffraction orders, can be captured simultaneously. As the object distance decreases, the images become clear from left to right.

The three-focus lens in this system results in an interval of 15 μm between adjacent two object planes, which can be calculated by Eq. (2). By means of the focus relay, the observation depth of the microscope can be up to 45 μm. Traditional optical microscope complicated with multi-focus image system can significantly improve the observation depth, which is critical for observing moving objects in real time.

4.2.2. Human blood smear

The imaging experiment with a small interval for human blood smear was carried out. Since the depth of field of a high-power objective is very shallow and the blood cells are distributed in different planes, a clear image for all cells cannot be obtained. By imaging multiple object planes with a proper interval and combining with subsequent image processing, a clear image with a large depth of field can be achieved [20,21].

In this experiment, the focal lengths of achromatic lens_1 and multi-focus diffraction lens are changed to 50 and 200 mm, respectively. The interval of object planes is 5 μm under the 50× objective. As shown in

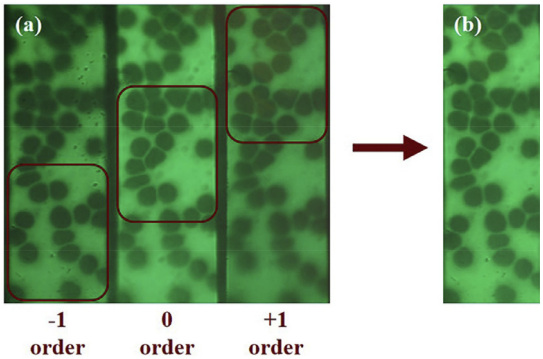

Fig. 8. Multi-focus imaging of human blood smear: (a) three independent images focused on different planes. (b) the clear image fused by multiple images.

Fig. 8(a), three images focused on different object planes are captured simultaneously with a single shot. The red boxes mark the focus of each image, in which the cells are clear. The remaining cells are blurred since they are out of the depth of field. As shown in Fig. 8(b), a clear image for all cells can be obtained by means of image processing methods such as focus stacking. This method can be combined with scanning microscope to record the information in parallel channels, which can greatly reduce the scanning time and improve the time resolution.

5. Conclusion

We have developed a broadband aberration-corrected multi-focus microscope based on the opposite dispersion between the diffraction and refraction elements. Simultaneous acquisition of multiple object planes of the sample can enlarge the observation depth and avoid the temporal inconsistence of sequentially recorded planes. A three-focus lens with two phase levels can obtain energy collection efficiency up to an optimum of 86.55%, and the nine-focus lens with three phase levels can get energy collection efficiency of 74.90%. For multi-focus lenses with focal length greater than 600 mm, the resolution reduction value can be controlled within 50 nm through achromatic measurement by rotating the fused silica ETP. Compared to the existing achromatic schemes, the method proposed in this paper has wider applicability according to the calculation and makes the system simpler. The multi-focus optical unit can deepen the observation range of conventional microscope, and improve the scanning efficiency and time resolution of scanning microscope. Owing to its ease of use, applicability to a series of multi-focus lens and excellent imaging performance, this method can facilitate the rapid acquisition of 3D data and real time observation for live cells in a wide range of depth.

Declaration of Competing Interest

The authors declare that they have no known competing financial interests or personal relationships that could have appeared to influence the work reported in this paper.

CRediT authorship contribution statement

Haidong Zhang: Conceptualization, Investigation, Methodology, Software, Writing - original draft. **Ruoqiu Wang:** Resources, Methodology, Software. **Xiaolin Yin:** Resources, Methodology, Software. **Xiaokun Wang:** Resources, Methodology, Software. **Xu Yang:** Supervision, Funding acquisition, Project administration. **Zhiyu Zhang:** Supervision, Funding acquisition, Writing - review & editing.

Acknowledgements

This work was supported by the Chinese Academy of Science (QYZDJ-SSW-JSC038, 181722KYSB20180015). This work was partially supported by the National Nature Science Foundation of China (51775531), Department of Science and Technology of Jilin Province (20180520202JH, 20200401065GX) and the China Scholarship Council (201804910813).

Supplementary materials

Supplementary material associated with this article can be found, in the online version, at doi:10.1016/j.optlaseng.2020.106283.

References

[1] Luo D, Taphanel M, Claus D, Boettcher T, Osten W, Längle T, et al. Area scanning method for 3D surface profilometry based on an adaptive confocal microscope. Opt Lasers Eng 2020:124. doi:10.1016/j.optlaseng.2019.105819.
[2] Zheng J, Zuo C, Gao P, Nienhaus GU. Dual-mode phase and fluorescence imaging with a confocal laser scanning microscope. Opt Lett 2018;43:5689. doi:10.1364/ol.43.005689.
[3] Hell SW, Sahl SJ, Bates M, Zhuang X, Heintzmann R, Booth MJ, et al. The 2015 super-resolution microscopy roadmap. J Phys D Appl Phys 2015:48. doi:10.1088/0022-3727/48/44/443001.
[4] Abrahamsson S, McQuilken M, Mehta SB, Verma A, Larsch J, Ilic R, et al. MultiFocus Polarization Microscope (MF-PolScope) for 3D polarization imaging of up to 25 focal planes simultaneously. Opt Express 2015;23:7734. doi:10.1364/oe.23.007734.
[5] Oudjedi L, Fiche J-B, Abrahamsson S, Mazenq L, Lecestre A, Calmon P-F, et al. Astigmatic multifocus microscopy enables deep 3D super-resolved imaging. Biomed Opt Express 2016;7:2163. doi:10.1364/boe.7.002163.
[6] Abrahamsson S, Usawa S, Gustafsson M. A new approach to extended focus for high-speed, high-resolution biological microscopy. Three-Dimensional Multidimens Microsc Image Acquis Process XIII 2006;6090:60900N. doi:10.1117/12.647022.
[7] Abrahamsson S, Ilic R, Wisniewski J, Mehl B, Yu L, Chen L, et al. Multifocus microscopy with precise color multi-phase diffractive optics applied in functional neuronal imaging. Biomed Opt Express 2016;7:855. doi:10.1364/boe.7.000855.
[8] Abrahamsson S, Blom H, Agostinho A, Jans DC, Jost A, Müller M, et al. Multifocus structured illumination microscopy for fast volumetric super-resolution imaging. Biomed Opt Express 2017;8:4135. doi:10.1364/BOE.8.004135.
[9] Lin W, Wang D, Meng Y, Chen SC. Multi-focus microscope with HiLo algorithm for fast 3-D fluorescent imaging. PLoS ONE 2019;14:1–13. doi:10.1371/journal.pone.0222729.
[10] Wisniewski J, Hajj B, Chen J, Mizuguchi G, Xiao H, Wei D, et al. Imaging the fate of histone Cse4 reveals de novo replacement in S phase and subsequent stable residence at centromeres. Elife 2014;2014:1–20. doi:10.7554/eLife.02203.
[11] Hajj B, Wisniewski J, El Beheiry M, Chen J, Revyakin A, Wu C, et al. Whole-cell, multicolor superresolution imaging using volumetric multifocus microscopy. Proc Natl Acad Sci U S A 2014;111:17480–5. doi:10.1073/pnas.1412396111.
[12] Ram S., Ward E.S., Ober R.J. 3D single molecule tracking and superresolution microscopy using multifocal plane microscopy. Proc - Int Symp Biomed Imaging 2012:914–5. 10.1109/ISBI.2012.6235702.
[13] Geissbuehler S, Sharipov A, Godinat A, Bocchio NL, Sandoz PA, Huss A, et al. Live-cell multiplane three-dimensional super-resolution optical fluctuation imaging. Nat Commun 2014;5:1–7. doi:10.1038/ncomms6830.
[14] Prabhat P, Ram S, Ward ES, Ober RJ. Simultaneous imaging of several focal planes in fluorescence microscopy for the study of cellular dynamics in 3D. Three-Dimensional Multidimens Microsc Image Acquis Process XIII 2006;6090:60900L. doi:10.1117/12.644343.
[15] Blanchard PM, Greenaway AH. Simultaneous multiplane imaging with a distorted diffraction grating. Appl Opt 1999;38:6692. doi:10.1364/ao.38.006692.
[16] Blanchard PM, Greenaway AH. Broadband simultaneous multiplane imaging. Opt Commun 2000;183:29–36. doi:10.1016/S0030-4018(00)00874-9.
[17] Abrahamsson S, Chen J, Hajj B, Stallinga S, Katsov AY, Wisniewski J, et al. Fast multicolor 3D imaging using aberration-corrected multifocus microscopy. Nat Methods 2013;10:60–3. doi:10.1038/NMETH.2277.
[18] Osipov V, Doskolovich LL, Bezus EA, Cheng W, Gaidukeviciute A, Chichkov B. Fabrication of three-focal diffractive lenses by two-photon polymerization technique. Appl Phys A Mater Sci Process 2012;107:525–9. doi:10.1007/s00339-012-6903-9.
[19] Doskolovich LL, Bezus EA, Morozov AA, Osipov V, Wolffsohn JS, Chichkov B. Multifocal diffractive lens generating several fixed foci at different design wavelengths. Opt Express 2018;26:4698. doi:10.1364/oe.26.004698.
[20] Yoo S, Ruiz P, Huang X, He K, Wang X, Gdor I, et al. Bayesian Approach for Automatic Joint Parameter Estimation in 3D Image Reconstruction from Multi-Focus Microscope. Proc - Int Conf Image Process ICIP 2018:3583–7. doi:10.1109/ICIP.2018.8451309.
[21] Yoo S, Ruiz P, Huang X, He K, Ferrier NJ, Hereld M, et al. 3D Image Reconstruction from Multi-Focus Microscope: axial Super-Resolution and Multiple-Frame Processing ICASSP, IEEE Int Conf Acoust Speech Signal Process - Proc 2018; 2018. -April:1453–7. doi:10.1109/ICASSP.2018.8462234.